

# SIDM on FIRE: Hydrodynamical Self-Interacting Dark Matter simulations of low-mass dwarf galaxies

Victor H. Robles<sup>1\*</sup>, James S. Bullock<sup>1</sup>, Oliver D. Elbert<sup>1</sup>, Alex Fitts<sup>2</sup>,  
Alejandro González-Samaniego<sup>1</sup>, Michael Boylan-Kolchin<sup>2</sup>, Philip F. Hopkins<sup>3</sup>,  
Claude-André Faucher-Giguère<sup>4</sup>, Dušan Kereš<sup>5</sup> and Christopher C. Hayward<sup>3,6</sup>

<sup>1</sup>Department of Physics and Astronomy, University of California, Irvine, CA 92697, USA

<sup>2</sup>Department of Astronomy, The University of Texas at Austin, 2515 Speedway, Stop C1400, Austin, TX 78712-1205, USA

<sup>3</sup>TAPIR, California Institute of Technology, Pasadena, CA, USA

<sup>4</sup>Department of Physics and Astronomy and CIERA, Northwestern University, Evanston, IL, USA

<sup>5</sup>Department of Physics, Center for Astrophysics and Space Sciences, University of California, San Diego, La Jolla, CA, USA

<sup>6</sup>Center for Computational Astrophysics, Flatiron Institute, 162 Fifth Avenue, New York, NY 10010, USA

26 June 2017

## ABSTRACT

We compare a suite of four simulated dwarf galaxies formed in  $10^{10}M_{\odot}$  haloes of collisionless Cold Dark Matter (CDM) with galaxies simulated in the same haloes with an identical galaxy formation model but a non-zero cross-section for dark matter self-interactions. These cosmological zoom-in simulations are part of the Feedback In Realistic Environments (FIRE) project and utilize the FIRE-2 model for hydrodynamics and galaxy formation physics. We find the stellar masses of the galaxies formed in Self-Interacting Dark Matter (SIDM) with  $\sigma/m = 1 \text{ cm}^2 \text{ g}^{-1}$  are very similar to those in CDM (spanning  $M_{\star} \approx 10^{5.7-7.0}M_{\odot}$ ) and all runs lie on a similar stellar mass – size relation. The logarithmic dark matter density slope ( $\alpha = d \log \rho / d \log r$ ) in the central 250 – 500 pc remains steeper than  $\alpha = -0.8$  for the CDM-Hydro simulations with stellar mass  $M_{\star} \sim 10^{6.6}M_{\odot}$  and core-like in the most massive galaxy. In contrast, every SIDM hydrodynamic simulation yields a flatter profile, with  $\alpha > -0.4$ . Moreover, the central density profiles predicted in SIDM runs without baryons are similar to the SIDM runs that include FIRE-2 baryonic physics. Thus, SIDM appears to be much more robust to the inclusion of (potentially uncertain) baryonic physics than CDM on this mass scale, suggesting SIDM will be easier to falsify than CDM using low-mass galaxies. Our FIRE simulations predict that galaxies less massive than  $M_{\star} \lesssim 3 \times 10^6 M_{\odot}$  provide potentially ideal targets for discriminating models, with SIDM producing substantial cores in such tiny galaxies and CDM producing cusps.

**Key words:** dark matter – galaxies: dwarf – galaxies: formation – Local Group

## 1 INTRODUCTION

The dark energy ( $\Lambda$ ) + cold dark matter (CDM) model assumes the dark matter is non-relativistic at decoupling and effectively collisionless, although it is weakly interacting with the standard model of particles.  $\Lambda$ CDM is in remarkable agreement with a variety of cosmological data on large scales (Komatsu et al. 2011; Planck Collaboration 2014), but its consistency with observations on the scale of dwarf galaxies is less clear. The predicted dense centers of CDM haloes are at the root of two of the most notable issues: the *cusp-core* problem states that inner density profiles of

dark-matter-dominated systems such as low mass and low surface brightness (LSB) galaxies appear to be cored, contrary to CDM-predicted cuspy centers (Moore 1994; Simon et al. 2005; Oh et al. 2011; Chan et al. 2015; Zhu et al. 2016; Kuzio de Naray & Kaufmann 2011; Kuzio de Naray & Spekkens 2011); and the *too big to fail* problem, which is that dark matter-only (DMO) simulations predict a substantial population of massive, centrally-concentrated subhaloes that does not appear to be present around the Milky Way (MW) or M31 (Boylan-Kolchin et al. 2011; Garrison-Kimmel et al. 2014).

These issues have driven substantial efforts to understand whether the discrepancies between theory and observations lie in an incomplete modeling of baryonic physics

\* E-mail: roblessv@uci.edu(UCI)

with the CDM paradigm. One particularly relevant prospect is the realization that bursty star formation, with accompanying violent gravitational potential fluctuations, may have the ability to re-shape the central gravitational potentials of even dark-matter-dominated systems (Governato et al. 2010; Governato et al. 2012; Pontzen & Governato 2012). Subsequent papers have shown that bursty star formation over an extended period can be effective in transforming a cusp to a core and in reducing the central densities of the DM halo (Oñorbe et al. 2015; Chan et al. 2015; Read et al. 2016; Tollet et al. 2016); additionally, baryonic physics could also help to alleviate the too big to fail problem (Chan et al. 2015; Wetzel et al. 2016; Zolotov et al. 2012). The results from existing CDM simulations of dwarf galaxies imply that variations in the SFH of a galaxy have a large impact on the associated DM halo, even when controlling for the host galaxy’s stellar mass (Oñorbe et al. 2015).

However, not all modern cosmological simulations of dwarf galaxies result in a cored density distribution for dwarf galaxies. Smoother star formation histories obtained via different assumptions for star formation (e.g., Sawala et al. 2016) lead to cuspy profiles. Even simulations that do result in feedback-induced cores typically find there is a limit to this process: as the halo mass decreases, decreased star formation efficiency renders core creation (on the scale of hundreds of parsecs) ineffective for galaxies with  $M_* \lesssim 10^6 M_\odot$  (Chan et al. 2015; Tollet et al. 2016; Fitts et al. 2016). Furthermore, properly addressing the problems found in low-mass galaxies ( $M_* \leq 10^9 M_\odot$ ) requires high-resolution simulations that can describe the central region of the dwarf DM haloes where these galaxies are hosted. Failure to resolve the dense centers of dwarfs can result in artificial cores in the DM profiles due to numerical artifacts (Garrison-Kimmel et al. 2013) that may be misinterpreted as core formation by stellar feedback in low-resolution hydrodynamical simulations.

If the addition of baryons is unable to fully address the small scale issues of CDM, it may be that there is actually no problem but rather it is an illusion caused by observational effects (as suggested by Pineda et al. (2017) and references therein); another approach is to consider different dark matter properties. Some alternative DM models are self-interacting dark matter (SIDM) (Spergel & Steinhardt 2000), ultra-light (scalar field/Bose-Einstein Condensate) dark matter (Sin 1994; Lee & Koh 1996; Guzmán & Matos 2000; Matos & Ureña López 2001; Robles & Matos 2013; Suárez et al. 2014; Mocz et al. 2017), and warm dark matter models (Lovell et al. 2014; Macciò et al. 2012). In this work, we focus on the SIDM model and consider the simplest option: identical dark-matter particles undergoing isotropic, velocity-independent, elastic, hard-sphere scattering with a cross section of  $\sigma$ . The scattering rate per particle scales as  $\Gamma(r) \sim \rho(r)(\sigma/m)v_{\text{rms}}$ , depending on the local mass density  $\rho$  and the r.m.s. speed of DM particles  $v_{\text{rms}}$ . Current constraints from DMO simulations of dwarf haloes that include self-interactions suggest that  $0.5 \text{ cm}^2 \text{ g}^{-1} < \sigma/m < 5 \text{ cm}^2 \text{ g}^{-1}$  can lead to cores of  $O(1 \text{ kpc})$  in their centers (Elbert et al. 2015; Fry et al. 2015) and thereby alleviating the CDM problems without the need of the baryonic component in dark matter dominated systems.

While the effects of baryons on CDM haloes and the effects of self-interactions in DMO simulations have been

examined extensively in the context of CDM’s small-scale “crisis”, much less work has explored the effects of baryonic physics and self-interactions simultaneously. Vogelsberger et al. (2014) and Fry et al. (2015) both found that galaxies with  $M_*(z=0) \approx 10^8 M_\odot$  simulated in SIDM with full hydrodynamics resulted in galaxies that were not appreciably different from CDM hydrodynamic (CDM-Hydro) simulations. However, it is not obvious that this is true at all stellar masses, as  $M_* \sim 10^8 M_\odot$  is near the peak of the core formation efficiency in CDM-Hydro simulations (Tollet et al. 2016; Chan et al. 2015; Di Cintio et al. 2014). It is especially interesting to consider systems with  $M_* \sim 10^5 - 10^6 M_\odot$ , as most theoretical work indicates such galaxies should retain their NFW cusps even when incorporating baryonic feedback (Fitts et al. (2016) and references therein).

In this paper, we address the robustness of SIDM predictions using simulations of a sample of 4 low-mass dwarf galaxies that incorporate realistic galaxy formation and stellar feedback models. The simulations are discussed in Section 2. In Section 3, we compare the results for the SIDM-DMO, CDM-DMO, and their corresponding hydrodynamical versions. Section 4 presents our main conclusions. We adopt a cosmological model with parameters  $\sigma_8 = 0.801$ ,  $\Omega_\Lambda = 0.734$ ,  $\Omega_m = 0.266$ ,  $\Omega_b = 0.0449$ ,  $n_s = 0.963$ , and  $h = 0.71$  (Komatsu et al. 2011) throughout this work.

## 2 SIMULATIONS

The starting point for our investigation is the cosmological hydrodynamical zoom-in simulations of Fitts et al. (2016). The Fitts et al. suite comprises 15 isolated haloes, with  $M_{\text{halo}}(z=0) \approx 10^{10} M_\odot$  and a diversity of assembly histories and  $z=0$  concentrations, chosen from periodic parent volumes with box sizes of 35 Mpc each. The simulations were all run as part of the FIRE<sup>1</sup> project (Hopkins et al. 2014) and adopt the FIRE-2 model (Hopkins et al. 2017). Accordingly, all of the simulations were performed with the GIZMO<sup>2</sup> code, and hydrodynamical versions use the mesh-free finite-mass (MFM) method in GIZMO. The high-resolution simulations have fixed gravitational softenings<sup>3</sup> of  $\epsilon_{\text{dm}} = 35 \text{ pc}$  for the DMO, and  $\epsilon_{\text{dm}} = 35 \text{ pc}$  and  $\epsilon_* = 3 \text{ pc}$  physical for the stars. The gas smoothing is fully adaptive and is the same for the hydrodynamic kernel and the gravitational softening; the minimum physical softening is  $h_{\text{gas}} = 1.4 \text{ pc}$ . The DM particle mass is  $m_{\text{dm}} \approx 3000 M_\odot$  for DMO and  $m_{\text{dm}} \approx 2500 M_\odot$  for Hydro runs;  $m_{\text{gas,initial}} \approx 500 M_\odot$  and the initial stellar mass is similar to the gas mass. At  $z=0$ , the haloes host galaxies with  $5.6 < \log_{10}(M_*/M_\odot) < 7.1$ .

From this suite, we have selected four haloes that span the full range of  $z=0$  stellar masses. Following the naming convention in Fitts et al. (2016), we resimulated haloes m10b, m10d, m10f, and m10k with a self-interaction cross section of  $\sigma/m = 1 \text{ cm}^2 \text{ g}^{-1}$  using the SIDM implementation of Rocha et al. (2013). This method considers interactions between pairs of phase-space patches, taking into account the collision term in the Boltzmann equation. For

<sup>1</sup> <http://fire.northwestern.edu>

<sup>2</sup> <http://www.tapir.caltech.edu/~phopkins/Site/GIZMO.html>

<sup>3</sup> We use the Plummer equivalent softening, the real region that is softened is  $2.8 \epsilon$ .

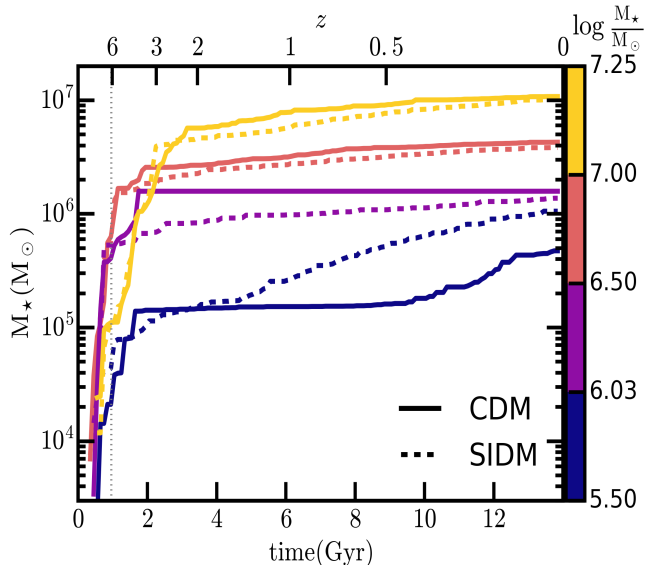


**Figure 1.** Evolution of the cumulative star formation history for each of our simulated galaxies. The four CDM galaxies (solid lines) are from the sample of [Fitts et al. \(2016\)](#), corresponding to: m10b (blue), m10d (purple), m10f (red), and m10f (yellow). Dashed-lines represent our SIDM simulations with the same initial conditions as the CDM haloes. Galaxies are colored according to their stellar mass at redshift  $z = 0$  (see [Table 1](#) for the exact values). We use the same color code in every figure. The dotted vertical line is where reionization ends in the simulations.

each halo simulated in SIDM, we perform a DMO version and a version with full FIRE-2 galaxy formation physics. Note that we therefore have 4 versions of each of the 4 haloes: CDM-DMO, CDM-Hydro, SIDM-DMO, and SIDM-Hydro. The implementation of galaxy formation physics is identical for all hydrodynamic runs (CDM and SIDM). Our high-resolution runs do not suffer from numerical relaxation for radii larger than 200 pc based on to the convergence criterion of [Power et al. \(2003\)](#); we adopt this value as our convergence radius in the density profiles. To identify the haloes in the simulations, we use the public code ROCKSTAR ([Behroozi et al. 2013](#)). We tested the robustness of the ROCKSTAR-determined centers using the Amiga Halo Finder code ([Knollmann & Knebe 2009](#)) and found no distinguishable differences in the converged region; for SIDM haloes, we found ROCKSTAR centers to be more accurate.

### 3 RESULTS

#### 3.1 Global Properties

Figure 1 shows the star formation histories of the four galaxies simulated in this work, with SIDM runs shown as dashed lines and their CDM counterparts shown as solid lines. These galaxies span the range of star formation histories in the [Fitts et al. \(2016\)](#) sample, which show a variety similar to those observed in nearby dwarf galaxies ([Skillman et al. 2014](#); [Cole et al. 2014](#)). The three most massive galaxies in CDM have very similar star formation histories in SIDM

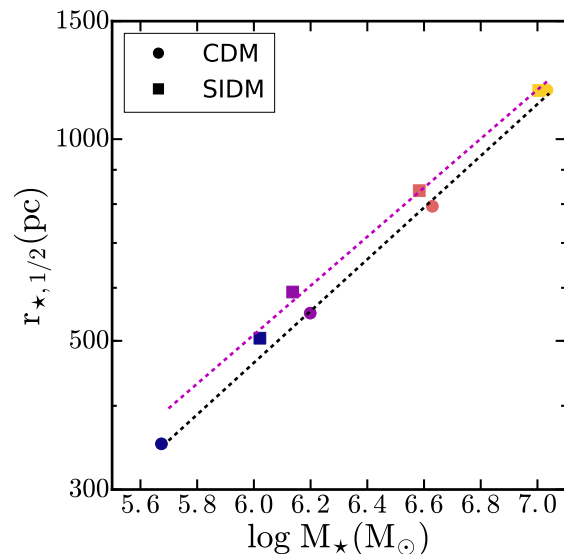


**Figure 2.** Effective 3D stellar half-mass radius vs total  $M_*$  within  $0.1 r_{\text{vir}}$  for the CDM (circles) and SIDM (squares) simulations. Note that the relationship for CDM galaxies and SIDM galaxies is very similar, with SIDM galaxies slightly larger at fixed stellar mass. The CDM galaxies are well fit by (dashed black line)  $r_{*,1/2}^{\text{cdm}} \propto (M_*^{\text{cdm}})^{0.386}$  while the SIDM galaxies follow a similar relation (dashed magenta line)  $r_{*,1/2}^{\text{sidm}} \propto (M_*^{\text{sidm}})^{0.365}$ .

(and very similar final  $M_*$ ). Only the lowest-mass halo exhibits a notable difference: while the CDM-Hydro simulation shows an extended pause in star formation from  $\sim 2$  Gyr to  $\sim 9$  Gyr of cosmic time, the SIDM-Hydro simulation forms stars continuously and ends up with twice as many stars at  $z = 0$ . It is not clear why these two galaxies show the most significant differences but it may be related to the enhanced sensitivity of star formation in small dwarfs that are most susceptible to UV background feedback ([Benítez-Llambay et al. 2017](#)); a detailed investigation of different types of feedback and their effects on galaxy formation in various dark matter models will be presented in future work.

The  $z = 0$  properties of our haloes and galaxies are summarized in [Table 1](#). Properties listed include the halo virial masses<sup>4</sup> at  $z = 0$  in each baryonic run, maximum circular velocities for both DMO and hydro runs, and the ratio of the virial mass in the hydrodynamic runs to those in the DMO runs. The ratio  $M_{\text{hydro}}/M_{\text{dmo}}$  is defined such that DMO virial mass assumes a loss of all baryonic matter:  $M_{\text{dmo}} = (1 - f_b)M_{\text{vir}}$ . We note that the quantities are generally fairly stable between the CDM and SIDM runs.

[Table 1](#) also lists the 3D stellar half-mass radius,  $r_{*,1/2}$ , for each galaxy. The relationship between stellar mass and galaxy  $r_{*,1/2}$  is plotted in [Figure 2](#). Results for CDM are shown as circles, while results for SIDM simulations are plotted as squares. Note that both dark matter models produce a similar stellar mass vs. galaxy size relationship. Even the lowest-mass halo, which forms twice as many stars in SIDM than in CDM, also falls on the stellar mass-size relation

<sup>4</sup> We define all virial quantities using the [Bryan & Norman \(1998\)](#) definition of the virial overdensity. For our chosen cosmology  $\Delta_{\text{vir}} = 96.45$  (relative to  $\rho_{\text{crit}}$  at  $z = 0$ ).

**Table 1.** Properties at  $z = 0$  for the simulated galaxies in CDM (values taken from [Fitts et al. \(2016\)](#)) and in SIDM. Columns: (1) Halo name used in the suite of [Fitts et al. \(2016\)](#); (2) Halo virial mass; (3) Maximum amplitude of the circular velocity; (4) Galaxy stellar mass (defined as  $M_\star(< 0.1 R_{\text{vir}})$ ); (5) 3D stellar half-mass radius; (6) Maximum of the circular velocity (DMO, after correction for cosmic baryon fraction  $f_b$ ); (7) Ratio of virial mass in hydro run to the virial mass in DMO run (DMO virial mass corrected for  $f_b$ ).

CDM						
Halo	$M_{\text{vir}}$ $M_\odot$	$V_{\text{max}}$ $\text{km s}^{-1}$	$M_\star$ $M_\odot$	$r_{\star,1/2}$ pc	$V_{\text{max}}^{\text{DMO}}$ $\text{km s}^{-1}$	$M_{\text{hydro}}/M_{\text{dmo}}$ –
m10b	$9.29 \times 10^9$	31.5	$4.65 \times 10^5$	340	34.8	0.96
m10d	$8.43 \times 10^9$	32.1	$1.53 \times 10^6$	530	37.6	0.98
m10f	$8.56 \times 10^9$	35.7	$4.11 \times 10^6$	750	41.2	0.94
m10k	$1.15 \times 10^{10}$	38.2	$1.04 \times 10^7$	1140	43.5	0.96
SIDM						
m10b	$8.13 \times 10^9$	30.8	$1.05 \times 10^6$	504	31.8	0.90
m10d	$8.10 \times 10^9$	33.1	$1.37 \times 10^6$	591	34.5	0.94
m10f	$8.39 \times 10^9$	35.7	$3.83 \times 10^6$	838	38.8	0.93
m10k	$1.12 \times 10^{10}$	37.6	$1.01 \times 10^7$	1260	40.4	0.94

in agreement with the rest of the simulations. In fact, all of the simulations, both CDM-Hydro and SIDM-Hydro, lie on a  $M_\star - r_{\star,1/2}$  relationship that is well approximated by  $r_{\star,1/2} \approx 456 \text{ pc} (M_\star/10^6 M_\odot)^{0.37}$ . Future work using different SIDM cross sections will reveal whether this similarity predicted by our galaxy size relation in SIDM and CDM holds beyond the specific cross section adopted here.

### 3.2 Density profiles

In Figure 3, we show the DM density profiles for all of our simulations. Each panel shows the DMO profiles<sup>5</sup> (thin lines) and hydro profiles (thick lines). In both cases, we plot results for CDM (solid) and SIDM (dashed) simulations. The arrow in each figure indicates the stellar half-mass radius ( $r_{\star,1/2}$ ) of the host galaxy. The galaxy that forms the lowest total stellar mass is shown in the upper left, while the most massive galaxy is shown in the bottom right panel. Fig. 3 shows that, in all cases, DMO simulations exhibit central density *cusps* in CDM (thin solid lines) and central density *cores* in SIDM (thin dotted lines).

Although all 4 haloes have nearly the same virial mass at  $z = 0$ , they have somewhat different assembly histories, leading to different concentrations and values of  $V_{\text{max}}$  ([Fitts et al. 2016](#)). These differences are further reflected in the core sizes seen in the SIDM-DMO runs in Fig. 3. The latest-forming, lowest-concentration haloes have lower central densities in CDM; lower central densities result in fewer DM interactions, as the interaction rate  $\Gamma$  scales as  $\Gamma \propto \rho(\sigma/m)v$ . Thus, the smaller  $V_{\text{max}}$  haloes end up with smaller SIDM-induced cores in the DMO runs.

As argued in [Fitts et al. \(2016\)](#), the more centrally-concentrated haloes are also the ones that form more stars in the CDM-Hydro runs, as they can accumulate more gas earlier and their central gravitational potentials are deeper, helping to offset the effects of later reionization feedback. In the CDM-Hydro runs, increasing the stellar mass also enhances core formation via star formation feedback. The density profile in the lowest-mass galaxy in the suite has no discernible difference when including hydrodynamics in CDM (upper left in Fig. 3); effects are still very small at  $M_\star \sim 10^6 M_\odot$  (upper right) but are beginning to become apparent when  $M_\star \sim 4 \times 10^6 M_\odot$  (lower left). The most massive galaxy (lower right), with  $M_\star \sim 10^7 M_\odot$ , has a pronounced density core in the CDM-Hydro run.

When including the effects of both galaxy formation and self-interactions, the situation changes both qualitatively and quantitatively. In all cases, the difference in density structure between SIDM-DMO and SIDM-Hydro simulations are relatively small, and the effects are smaller than in the equivalent CDM-Hydro runs in every case. The largest effects for SIDM-Hydro are seen in the most massive galaxy, where the core density is reduced by  $\sim 40\%$  relative to the SIDM-DMO run (the core radius remains the same). Even though our lowest-mass and highest-mass galaxies in SIDM-Hydro differ by a factor of 10 in stellar mass, their profiles show much smaller differences with respect to their SIDM-DMO runs in contrast to the CDM-hydro vs CDM-DMO results.

Figure 4 highlights the differences between CDM and SIDM as a function of galaxy stellar mass by showing only the hydro density profiles (solid for CDM, dotted for SIDM). In the left panels, we plot the density profiles for the three lowest stellar mass systems, while the right panel shows the density profile of the highest stellar mass galaxy. Only the galaxy with the highest stellar mass ( $M_\star = 10^7 M_\odot$ , right panel) forms a core in the CDM runs, while all galaxies have

<sup>5</sup> DMO density profiles are corrected for the cosmic baryon fraction as in [Fitts et al. \(2016\)](#).

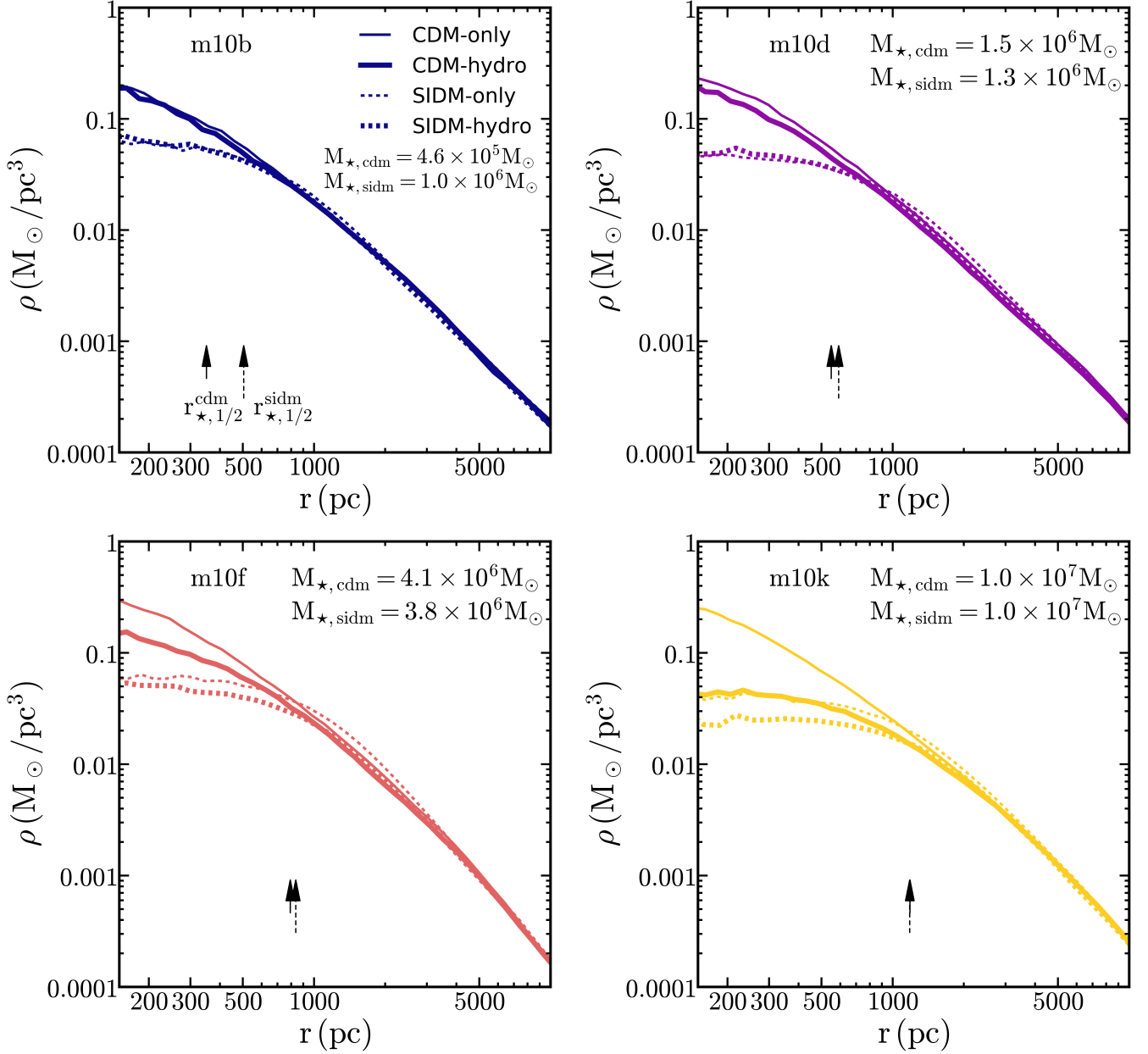


**Figure 3.** Dark matter density profiles for the four SIDM (dashed lines) and CDM (solid lines) simulations. Profiles of the hydrodynamical simulations with the FIRE physics are shown with thick lines and dark matter-only (DMO) simulations are shown with thin lines. Also shown with arrows in each panel are the effective stellar mass radii ( $r_{*,1/2}$ ). The colors are the same as in Fig.1; each panel is labeled with the name of the halo and its stellar mass at  $z = 0$  in both dark matter models (see Table 1 for a summary of the individual properties.)

sizable cores in the SIDM versions. In all three of the lower stellar mass systems, the central dark matter properties are primarily determined by the dark matter physics, with baryonic effects playing a minimal role. It is only in the highest  $M_*$  galaxy that baryons significantly alter the structure in the CDM halo (and further reduce the density in the SIDM). This result further strengthens the picture in which galaxies with  $M_* \lesssim 3 \times 10^6 M_\odot$  have dark matter density profiles that are essentially unmodified by baryons (Oñorbe et al. 2015; Chan et al. 2015; Tollet et al. 2016).

### 3.3 Density profile slopes

Results in the previous subsection demonstrate that feedback can reduce the central dark matter density in CDM halos, provided enough stars form. The same subsection also demonstrates that SIDM alone can do so as well. However, the precise nature of this reduction is important, and in this subsection, we study the slopes of the density profiles quantitatively. We obtain the inner slope of the DM density assuming a power law and apply the  $\chi^2$  fitting method to the density profiles within 250-500 pc range, which is comparable to 0.5-1% the virial radii of their DM haloes.

Figure 5 shows the resulting logarithmic slope  $\alpha(r) =$

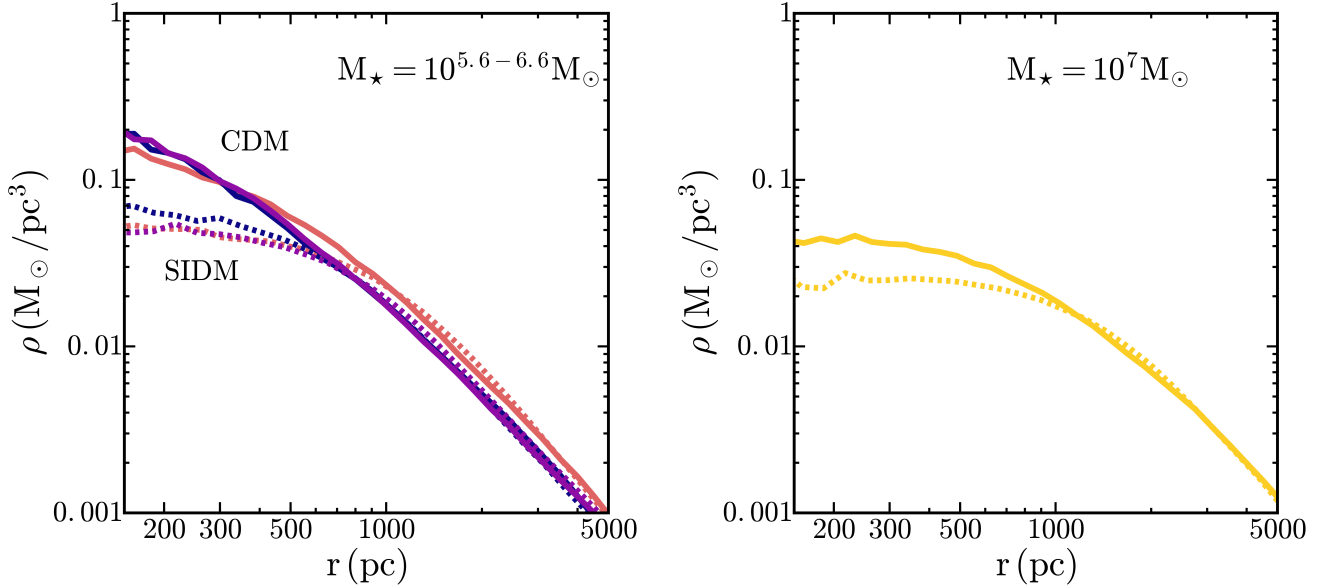


**Figure 4.** Dark matter density profiles for our FIRE-2 hydro simulations that form  $M_* = 10^{5.6-6.6}M_\odot$  (left panel) and for the most massive galaxy ( $M_* = 10^7M_\odot$ ; right panel). Dwarf galaxy haloes in CDM retain their cusp for  $M_* < 10^{6.6}M_\odot$ ; only in our most massive galaxy both CDM and SIDM display a large core ( $\sim 1$  kpc).

$d \log \rho / d \log r$  of the hydro (filled symbols) and DMO (empty symbols) simulations as a function of the stellar mass of the galaxy (top row). Also shown is the slope of the profiles versus radial distance from the halo centers (bottom row), with arrows marking the stellar half-mass radii for each halo. For the estimation of the central slope, we varied the fitting range and the bin size and found slopes that do not differ by more than 0.1 dex; this uncertainty is accounted for by the size of the symbols in the figure. We find that only one of the CDM-Hydro simulations in our sample truly becomes “cored” (defined here as  $\alpha > -0.3$ ), and even then, this happens only at very small radii ( $r \lesssim 300$  pc). As the stellar mass of the galaxies decreases, the inner slopes in the CDM-Hydro simulations decrease to the mild-cusp  $-0.6 \leq \alpha < -0.3$  and to the cuspy region ( $\alpha < -0.6$ ). The cuspy inner slopes in the CDM-DMO runs remain largely unaffected by stellar feedback from FIRE for galaxies with  $\log M_*/M_\odot < 6.2$  and have only a mild change for the galaxy with  $\log M_*/M_\odot \sim 6.6$ .

In contrast, all SIDM simulations (DMO and Hydro) exhibit central density cores. Despite varying in an order of magnitude in  $M_*$ , the SIDM-Hydro simulations all have central density profiles with slopes of  $\alpha > -0.5$ . More importantly, the slopes in the hydro runs closely follow their DMO values, even for the highest stellar masses. The close similarity between the density profiles of the SIDM-DMO and SIDM-Hydro runs – including the similar shape of  $\alpha(r)$  across all values of  $M_*$  – indicates that independently of the galaxy mass and SFH, core formation and reduction of central densities in SIDM simulations are set mainly by dark matter physics rather than by galaxy formation physics (for the cross section  $\sigma/m = 1 \text{ cm}^2 \text{ g}^{-1}$  studied here). This provides a striking contrast to the major role that feedback plays in forming cores in CDM simulations. In fact, the stellar mass dependence of the density profile slope in CDM-Hydro simulations is seen at radii of up to  $\sim 1$  kpc.

*SIDM predictions regarding the central gravitational potential of  $M_* \sim 10^6 M_\odot$  dwarf galaxies appear relatively robust to the effects of stellar feedback, while CDM predictions depend sensitively on it.*

The changes in DM densities found in SIDM-Hydro versus CDM-Hydro simulations are quantified in more detail in Figure 6, which shows the difference in  $\alpha(r)$  between these runs. For the same FIRE physics, the SIDM densities are more than 25% different from the CDM densities for  $r < 500$  pc (and can be over 50% different at 250 pc). This ratio shows little dependence on  $M_*$ . The left panel shows that less massive galaxies exhibit larger differences in the slope, with the largest change happening within the SIDM half-mass radii (where self-interactions form the core). The smallest difference in the slope occurs for the most massive galaxy, as feedback in the CDM version of this halo is strong enough to create a core similar to its SIDM analog.

### 3.4 Shapes

Many studies have shown that CDM haloes in DMO simulations are triaxial (Vega-Ferrero et al. 2017; Schneider et al. 2012; Springel et al. 2004). SIDM haloes are expected to be closer to spherical in the region for which self-interactions are important, as the interactions tend to isotropize the density distribution (Spergel & Steinhardt 2000; Kaplinghat et al. 2014; Rocha et al. 2013; Peter et al. 2013; Zavala et al. 2013; Elbert et al. 2015). The shapes of low-mass dark matter haloes and their dwarf galaxies may therefore contain important clues about the nature of dark matter.

We show a visualization of the DM distribution corresponding to one of our simulations (m10d in Table 1) in Figure 7. The SIDM-DMO run indeed exhibits a distinctive roundness within the half-mass radius ( $\sim 1$  kpc), while the CDM-DMO run is noticeably more triaxial. In both mod-

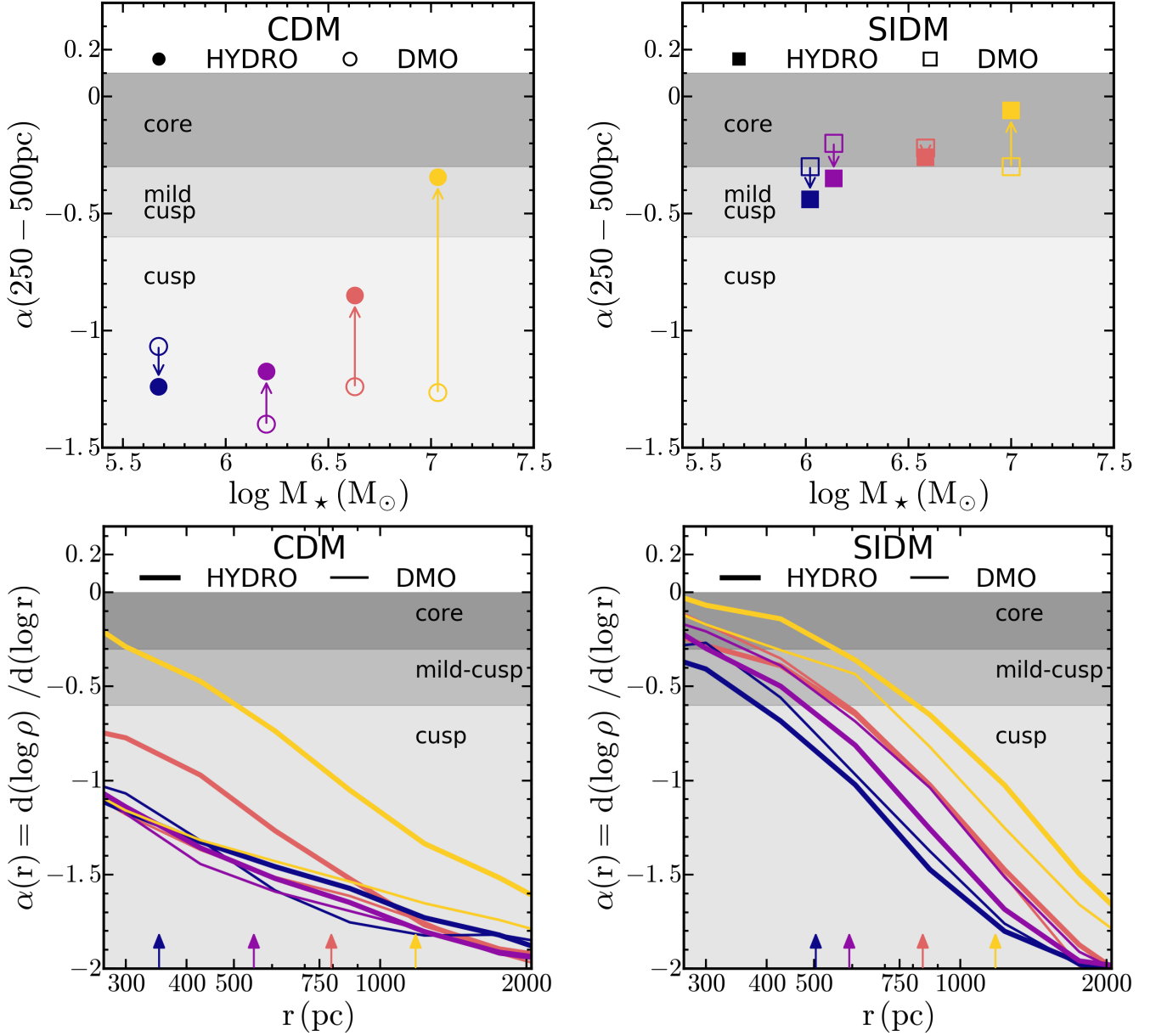


**Figure 5.** Upper row: slopes of DM density  $\alpha$  as a function of halo mass for the simulated CDM haloes (left column) and SIDM haloes (right column). The slopes were obtained by fitting the DM density profiles in the range 250 – 500 pc ( $0.5 - 1\% r_{\text{vir}}$ ). Filled symbols correspond to simulated haloes with FIRE and empty symbols are with DMO, for the latter we used the same stellar mass (and color) as their hydro simulation for an easier comparison of the slopes. Lower row: slope of DM density vs radius for CDM (left column) and SIDM (right column) haloes, thick lines represent the simulations with FIRE and thin lines the DMO ones (we use the same color for the respective DMO run). The arrows at the bottom mark the effective half-mass radius,  $r_{\star, 1/2}$ , for its associated hydro simulation (identified by the same color of the arrow). The horizontal dark gray region is where the density profile is flat enough so that we call it a core ( $-0.3 \leq \alpha < 0.1$ ), below (light gray) is the mild-cusp region ( $-0.6 \leq \alpha < -0.3$ ) and at the bottom is the cusp region ( $\alpha < -0.6$ ).

els, the inclusion of hydrodynamics mildly affects the DMO predictions.

To characterize halo shapes, we compute shape tensors using an iterative method (Dubinski & Carlberg 1991; Zemp et al. 2011). The shape tensor eigenvalues are proportional to the square root of the principal axes of the ellipsoid that characterize the particle distribution. Following the standard nomenclature for the semi-principal axes  $a$ ,  $b$  and  $c$ , we choose  $a \geq b \geq c$  and calculate the axis ratios  $b/a$  and  $c/a$ . In general,  $c/a$  and  $b/a$  quantify the degree of triaxiality

of the distribution under study, because  $c$  is the smallest of the semi-principal axes, then  $c/a \approx 1$  will imply  $b/a$  is also close to unity and any deviations from spherical symmetry will be small.

Table 2 summarizes the axis ratios  $b/a$  and  $c/a$  for the central DM distribution using the particles within 1 kpc for each of the haloes. For the hydrodynamical simulations, we also include the axis ratios of the stars within the same radius. We can assess the effect of the dark matter properties and/or the feedback on the shape of the inner DM mass dis-

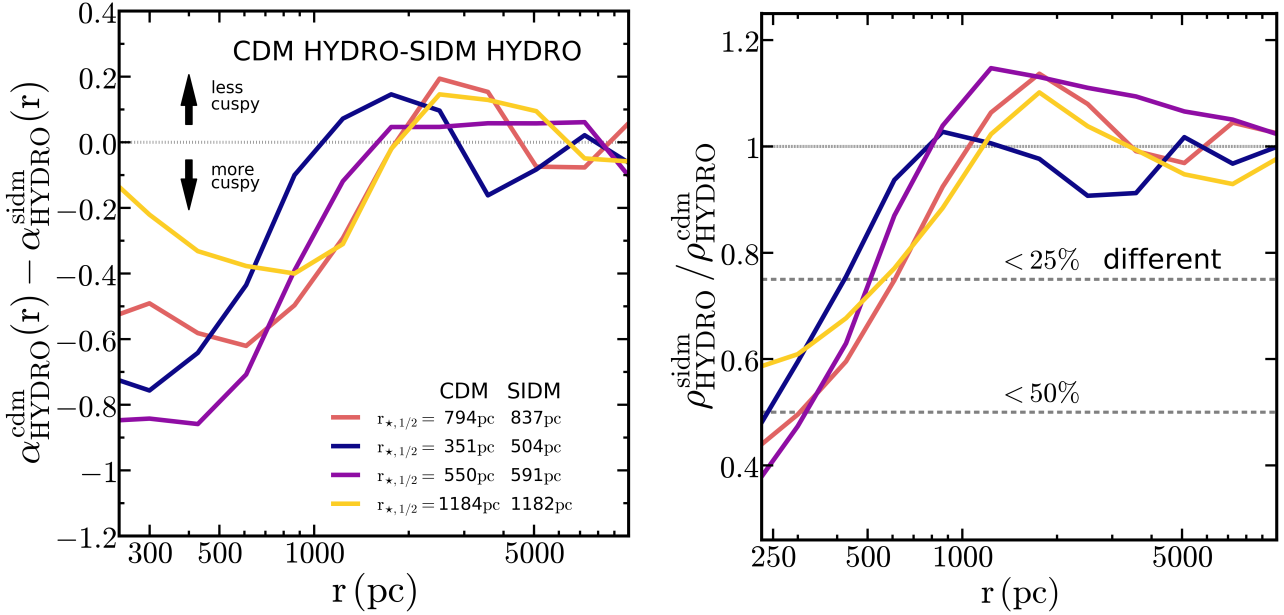


**Figure 6.** Left: Relative change of the DM density slope between the CDM and SIDM-Hydro simulations vs radius. The largest difference appears in the most massive galaxy starting at the effective stellar radius ( $r_{*,1/2}$ ), this is also seen for the other galaxies at their respective  $r_{*,1/2}$ , as can be inferred from their values in the labels. Right: Dark matter density ratio of the SIDM-Hydro simulation and its CDM-Hydro pair. The gray dashed lines show the transition limit above which the ratio of the density profiles differs in less than < 25% and < 50%, respectively. SIDM galaxies become less dense towards the center reaching a  $\geq 25\%$  difference from their CDM counterparts at  $\sim 500$  pc.

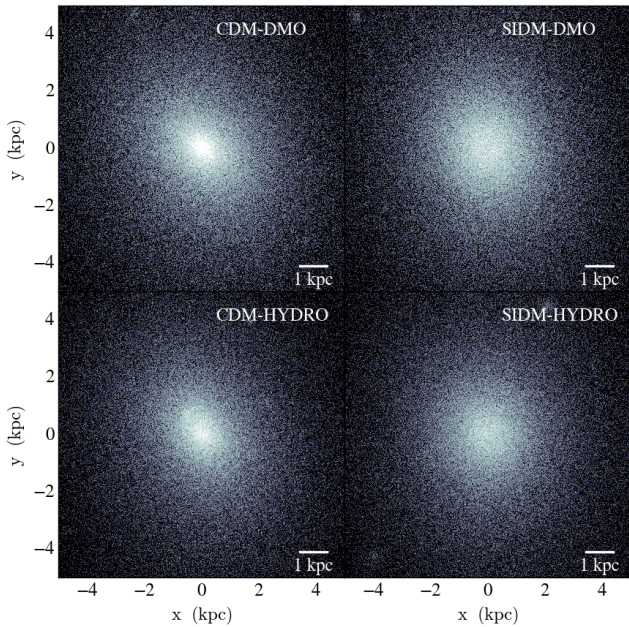


**Figure 7.** Projected  $(x-y)$  plane visualization of the dark matter within a 5 kpc radius from the center for m10f ( $M_{*,\text{cdm}} \approx 4.11 \times 10^6 M_{\odot}$ ). The galaxy ends with roughly equal stellar mass in both DM models, the FIRE-2 baryonic physics reduces the central dark matter density for the CDM-Hydro simulation compared to the DMO, whereas the same feedback physics has a milder effect in the SIDM-Hydro simulation.

tribution in dwarf galaxies<sup>6</sup> by computing the 3D-axis ratios at the typical size of the visible matter in dwarf galaxies for the Hydro and DMO runs in both DM models.

We find a systematic preference for the cuspy CDM haloes (both DMO and Hydro) to be triaxial: even the galaxy with a core (m10k) is less round (lower  $c/a$  ratio) than any of the SIDM haloes. While the galaxy formation physics in the FIRE-2 model affects the inner shapes of the halos in SIDM-Hydro runs, those halos remain rounder than the versions in the CDM-Hydro runs. The galaxies formed in both cases are fairly triaxial, though the SIDM galaxies are slightly closer to spherical. Galaxy formation physics (as opposed to gravitational physics or self-interactions) therefore appears to play the dominant role in establishing shapes of dwarf galaxies in these simulations.

#### 4 DISCUSSION AND CONCLUSIONS

SIDM preserves the successes of  $\Lambda$ CDM on large scales while simultaneously providing a path to ameliorate small-scale challenges to the model (Bullock & Boylan-Kolchin 2017). The main effect of SIDM on dark matter haloes is to reduce the density and sphericalize the dark matter distribution on scales where many dark matter self-interactions can occur per Hubble time (Elbert et al. 2015; Rocha et al. 2013;

<sup>6</sup> It is important to note that we are measuring the triaxial distribution for particles within 1 kpc where the feedback has the largest effect on the DM; the results are unchanged if we consider the axis ratios at 0.5 kpc or 1.5 kpc rather than at 1 kpc. The values presented in Table 1 are only meant to characterize the shape of the inner region of the halo, not its entire extent.



**Table 2.** 3D-axis ratio between the smallest and the largest semi-principal axis ( $c/a$ ) of the DM and of the stellar mass distributions computed at 1 kpc. Columns: (1) Halo name used in the suite of [Fitts et al. \(2016\)](#); (2)-(9) DM axis ratios ( $b/a$  and  $c/a$ ) for each of the 4 simulations for both cases, DMO and DM+Hydro, as indicated by the column labels. Columns (10)-(13) show the 3D-axis ratios ( $b/a$  and  $c/a$ ) for the stellar component in CDM and SIDM, respectively, also calculated at 1 kpc.

Halo	Dark Matter-Only (DMO)				DM+Hydro				Stars			
	CDM		SIDM		CDM		SIDM		CDM		SIDM	
	$b/a$	$c/a$	$b/a$	$c/a$	$b/a$	$c/a$	$b/a$	$c/a$	$b/a$	$c/a$	$b/a$	$c/a$
m10b	0.50	0.38	0.90	0.76	0.55	0.43	0.80	0.68	0.58	0.49	0.70	0.43
m10d	0.57	0.44	0.87	0.84	0.56	0.44	0.85	0.76	0.63	0.49	0.81	0.65
m10f	0.52	0.42	0.95	0.91	0.57	0.43	0.88	0.79	0.60	0.46	0.69	0.56
m10k	0.55	0.41	0.94	0.85	0.60	0.45	0.81	0.72	0.60	0.45	0.67	0.51

[Kaplinghat et al. 2014](#); [Kaplinghat et al. 2016](#)). In order to understand *observable* consequences of SIDM, however, we must study the combined effects of SIDM and galaxy formation physics.

In this paper, we present high-resolution SIDM cosmological simulations (with  $\sigma/m = 1 \text{ cm}^2 \text{ g}^{-1}$ ) of four isolated dwarf galaxies taken from a large suite of  $M_{\text{halo}}(z=0) \approx 10^{10} M_{\odot}$  haloes ([Fitts et al. 2016](#)). In each case, we have dark-matter-only and hydrodynamical simulations; the hydrodynamical simulations employ an identical model of galaxy formation physics (FIRE-2) to the CDM versions of the haloes presented in [Fitts et al. \(2016\)](#). Accordingly, we are able to understand the modification of halo properties due to dark matter self-interactions alone (by comparing CDM-DMO and SIDM-DMO runs) and modifications coming from a combination of dark matter physics and galaxy formation physics (by comparing both hydro runs). The high spatial and mass resolution of our simulations allow us to unambiguously address the impact of stellar feedback on the core formation and density reduction within 1 kpc of each of the SIDM and CDM galaxies.

We focus on the comparison of DM profiles in DMO and hydro simulations for the SIDM and CDM models. We show that SIDM galaxies display similar star formation histories as their CDM counterparts, resulting in nearly identical stellar masses and sizes in each case. The sole exception is the lowest-mass galaxy, which forms twice as many stars in SIDM but it nonetheless follows the same stellar mass - size relation as rest of the sample, which is essentially identical in CDM and SIDM (see [Figure 2](#)).

In the CDM simulations, the main mechanism to modify a central dark matter cusp is stellar feedback. As demonstrated by [Fitts et al. \(2016\)](#), the effects of stellar feedback at the halo mass scale considered here –  $10^{10} M_{\odot}$  – are strongly dependent on stellar mass (see also [Chan et al. \(2015\)](#); [Tollet et al. \(2016\)](#); [Oñorbe et al. \(2015\)](#)). Galaxies with  $M_{\star} \lesssim 3 \times 10^6 M_{\odot}$  maintain the central cusp found in DMO runs, while those with  $M_{\star} \gtrsim 3 \times 10^6 M_{\odot}$  have reduced central densities, with the reduction increasing with stellar mass. SIDM produces qualitatively different results: the central densities in DMO simulations are reduced significantly through dark matter self-interactions. When considering the change between DMO and hydro runs in SIDM, however, differences are minimal: the dark matter core sizes and density

profiles in the full physics runs are generically very similar to their DMO counterparts. *Feedback only has a minimal effect on the dark matter structure of SIDM dwarf galaxies over the mass range simulated here ( $10^6 \lesssim M_{\star}/M_{\odot} \lesssim 10^7$ ).*

Based on our results, the discovery of dark matter cores on the scale of  $r_{1/2}$  in field dwarf galaxies with  $M_{\star} \lesssim 3 \times 10^6 M_{\odot}$  would imply one of the following: (1) dark matter is cold but the implementation of astrophysical processes in current codes is incomplete; (2) there is a large scatter in the halo masses of dwarf galaxies with  $M_{\star} \lesssim 3 \times 10^6 M_{\odot}$ ; or (3) dark matter has physics beyond that of a cold and collisionless thermal relic – perhaps self-interactions of the kind explored here. The shape of the dark matter density profiles in  $M_{\star} \sim 10^6 M_{\odot}$  isolated dwarf galaxies on scales comparable to the galaxy half-mass radius therefore provide a crucial test of dark matter models.

## ACKNOWLEDGEMENTS

V.H.R. acknowledges support from UC-MEXUS and CONACyT through the postdoctoral fellowship. A.G-S. acknowledges support from UC-MEXUS through the postdoctoral Fellowship. JSB is supported by NSF and HST grants at UC Irvine. MBK acknowledges support from NSF grant AST-1517226 and from NASA grants NNX17AG29G and HST-AR-12836, HST-AR-13888, HST-AR-13896, and HST-AR-14282 from the Space Telescope Science Institute, which is operated by AURA, Inc., under NASA contract NAS5-26555. DK was supported by NSF grant AST-1412153 and the Cottrell Scholar Award from the Research Corporation for Science Advancement. CAFG was supported by NSF through grants AST-1412836 and AST-1517491, and by NASA through grant NNX15AB22G. Our simulations used computational resources provided via the NASA Advanced Supercomputing (NAS) Division and the NASA Center for Climate Simulation (NCCS) and the Extreme Science and Engineering Discovery Environment, which is supported by National Science Foundation grant number OCI-1053575.

## REFERENCES

- Behroozi P. S., Wechsler R. H., Wu H.-Y., 2013, *ApJ*, **762**, 109  
 Benítez-Llambay A., et al., 2017, *MNRAS*, **465**, 3913

- Boylan-Kolchin M., Bullock J. S., Kaplinghat M., 2011, *MNRAS*, **415**, L40
- Bryan G. L., Norman M. L., 1998, *ApJ*, **495**, 80
- Bullock J. S., Boylan-Kolchin M., 2017, *Annual Review of Astronomy and Astrophysics*, 55
- Chan T. K., Kereš D., Oñorbe J., Hopkins P. F., Muratov A. L., Faucher-Giguère C.-A., Quataert E., 2015, *MNRAS*, **454**, 2981
- Cole A., Weisz D. R., Dolphin A. E., Skillman E., McConnachie A., Brooks A. M., Leaman R., 2014, *The Astrophysical Journal*, **795**, 54
- Di Cintio A., Brook C. B., Macciò A. V., Stinson G. S., Knebe A., Dutton A. A., Wadsley J., 2014, *MNRAS*, **437**, 415
- Dubinski J., Carlberg R. G., 1991, *ApJ*, **378**, 496
- Elbert O. D., Bullock J. S., Garrison-Kimmel S., Rocha M., Oñorbe J., Peter A. H. G., 2015, *MNRAS*, **453**, 29
- Fitts A., et al., 2016, preprint, ([arXiv:1611.02281](https://arxiv.org/abs/1611.02281))
- Fry A. B., et al., 2015, *MNRAS*, **452**, 1468
- Garrison-Kimmel S., Rocha M., Boylan-Kolchin M., Bullock J. S., Lally J., 2013, *MNRAS*, **433**, 3539
- Garrison-Kimmel S., Boylan-Kolchin M., Bullock J. S., Kirby E. N., 2014, *MNRAS*, **444**, 222
- Governato F., et al., 2010, *Nature*, **463**, 203
- Governato F., et al., 2012, *MNRAS*, **422**, 1231
- Guzmán F. S., Matos T., 2000, *Classical and Quantum Gravity*, **17**, L9
- Hopkins P. F., Kereš D., Oñorbe J., Faucher-Giguère C.-A., Quataert E., Murray N., Bullock J. S., 2014, *MNRAS*, **445**, 581
- Hopkins P. F., et al., 2017, preprint, ([arXiv:1702.06148](https://arxiv.org/abs/1702.06148))
- Kaplinghat M., Keeley R. E., Linden T., Yu H.-B., 2014, *Physical Review Letters*, **113**, 021302
- Kaplinghat M., Tulin S., Yu H.-B., 2016, *Phys. Rev. Lett.*, **116**, 041302
- Knollmann S. R., Knebe A., 2009, *ApJS*, **182**, 608
- Komatsu E., et al., 2011, *ApJS*, **192**, 18
- Kuzio de Naray R., Kaufmann T., 2011, *MNRAS*, **414**, 3617
- Kuzio de Naray R., Spekkens K., 2011, *The Astrophysical Journal Letters*, **741**, L29
- Lee J.-W., Koh I.-G., 1996, *Phys. Rev. D*, **53**, 2236
- Lovell M. R., Frenk C. S., Eke V. R., Jenkins A., Gao L., Theuns T., 2014, *MNRAS*, **439**, 300
- Macciò A. V., Paduroiu S., Anderhalden D., Schneider A., Moore B., 2012, *MNRAS*, **424**, 1105
- Matos T., Ureña López L., 2001, *Phys. Rev. D*, **63**, 063506
- Mocz P., Vogelsberger M., Robles V. H., Zavala J., Boylan-Kolchin M., Hernquist L., 2017, preprint, ([arXiv:1705.05845](https://arxiv.org/abs/1705.05845))
- Moore B., 1994, *Nature*, **370**, 629
- Oñorbe J., Boylan-Kolchin M., Bullock J. S., Hopkins P. F., Kereš D., et al. 2015, *MNRAS*, **454**, 2092
- Oh S.-H., Brook C., Governato F., Brinks E., Mayer L., de Blok W. J. G., Brooks A., Walter F., 2011, *The Astronomical Journal*, **142**, 24
- Peter A. H. G., Rocha M., Bullock J. S., Kaplinghat M., 2013, *MNRAS*, **430**, 105
- Pineda J. C. B., Hayward C. C., Springel V., Mendes de Oliveira C., 2017, *Monthly Notices of the Royal Astronomical Society*, **466**, 63
- Planck Collaboration 2014, *A&A*, **571**, A16
- Pontzen A., Governato F., 2012, *MNRAS*, **421**, 3464
- Power C., Navarro J. F., Jenkins A., Frenk C. S., White S. D. M., Springel V., Stadel J., Quinn T., 2003, *MNRAS*, **338**, 14
- Read J. I., Agertz O., Collins M. L. M., 2016, *MNRAS*, **459**, 2573
- Robles V. H., Matos T., 2013, *ApJ*, **763**, 19
- Rocha M., Peter A. H. G., Bullock J. S., Kaplinghat M., Garrison-Kimmel S., Oñorbe J., Moustakas L. A., 2013, *MNRAS*, **430**, 81
- Sawala T., et al., 2016, *MNRAS*, **457**, 1931
- Schneider M. D., Frenk C., S. C., 2012, *Journal of Cosmology and Astroparticle Physics*, 2012, 030
- Simon J. D., Bolatto A., Leroy A., Blitz L., Gates E. L., 2005, *ApJ*, **621**, 757
- Sin S.-J., 1994, *Phys. Rev. D*, **50**, 3650
- Skillman E., et al., 2014, *The Astrophysical Journal*, **786**, 44
- Spergel D. N., Steinhardt P. J., 2000, *Phys. Rev. Lett.*, **84**, 3760
- Springel V., White S. D. M., Hernquist L., 2004, in Ryder S., Pisano D., Walker M., Freeman K., eds, *IAU Symposium Vol. 220, Dark Matter in Galaxies*. p. 421
- Suárez A., Robles V. H., Matos T., 2014, in Moreno González C., Madriz Aguilar J. E., Reyes Barrera L. M., eds, *Astrophysics and Space Science Proceedings Vol. 38, Accelerated Cosmic Expansion*. p. 107 ([arXiv:1302.0903](https://arxiv.org/abs/1302.0903)), doi:10.1007/978-3-319-02063-1\_9
- Tollet E., et al., 2016, *MNRAS*, **456**, 3542
- Vega-Ferrero J., Yepes G., Gottlöber S., 2017, *MNRAS*, **467**, 3226
- Vogelsberger M., Zavala J., Simpson C., Jenkins A., 2014, *MNRAS*, **444**, 3684
- Wetzel A. R., Hopkins P., Kim J.-h., Faucher-Giguère C., Kereš D., Quataert E., 2016, *The Astrophysical Journal Letters*, **827**, L23
- Zavala J., Vogelsberger M., Walker M. G., 2013, *MNRAS: Letters*, **431**, L20
- Zemp M., Gnedin O. Y., Gnedin N., Kravtsov A., 2011, *The Astrophysical Journal Supplement Series*, **197**, 30
- Zhu Q., Marinacci F., Maji M., Li Y., Springel V., Hernquist L., 2016, *MNRAS*, **458**, 1559
- Zolotov A., et al., 2012, *The Astrophysical Journal*, **761**, 71

This paper has been typeset from a  $\text{\TeX}/\text{\LaTeX}$  file prepared by the author.